

RESEARCH

Open Access



Momordicine-I suppresses head and neck cancer growth by modulating key metabolic pathways

Debojyoty Bandyopadhyay¹, Ellen T. Tran¹, Ruchi A. Patel¹, Matthew A. Luetzen², Kevin Cho^{3,4}, Leah P. Shriver^{3,4}, Gary J. Patti^{3,4}, Mark A. Varvares⁵, David A. Ford², Kyle S. McCommis² and Ratna B. Ray^{1*}

Abstract

One of the hallmarks of cancer is metabolic reprogramming which controls cellular homeostasis and therapy resistance. Here, we investigated the effect of momordicine-I (M-I), a key bioactive compound from *Momordica charantia* (bitter melon), on metabolic pathways in human head and neck cancer (HNC) cells and a mouse HNC tumorigenicity model. We found that M-I treatment on HNC cells significantly reduced the expression of key glycolytic molecules, *SLC2A1* (GLUT-1), *HK1*, *PFKP*, *PDK3*, *PKM*, and *LDHA* at the mRNA and protein levels. We further observed reduced lactate accumulation, suggesting glycolysis was perturbed in M-I treated HNC cells. Metabolomic analyses confirmed a marked reduction in glycolytic and TCA cycle metabolites in M-I-treated cells. M-I treatment significantly downregulated mRNA and protein expression of essential enzymes involved in de novo lipogenesis, including *ACLY*, *ACC1*, *FASN*, *SREBP1*, and *SCD1*. Using shotgun lipidomics, we found a significant increase in lysophosphatidylcholine and phosphatidylcholine loss in M-I treated cells. Subsequently, we observed dysregulation of mitochondrial membrane potential and significant reduction of mitochondrial oxygen consumption after M-I treatment. We further observed M-I treatment induced autophagy, activated AMPK and inhibited mTOR and Akt signaling pathways and leading to apoptosis. However, blocking autophagy did not rescue the M-I-mediated alterations in lipogenesis, suggesting an independent mechanism of action. M-I treated mouse HNC MOC2 cell tumors displayed reduced *Hk1*, *Pdk3*, *Fasn*, and *Acly* expression. *In conclusion*, our study revealed that M-I inhibits glycolysis, lipid metabolism, induces autophagy in HNC cells and reduces tumor volume in mice. Therefore, M-I-mediated metabolic reprogramming of HNC has the potential for important therapeutic implications.

Keywords Momordicine-I, Head and neck cancer, Glycolysis, Lipid metabolism, Metabolites, Autophagy

*Correspondence:

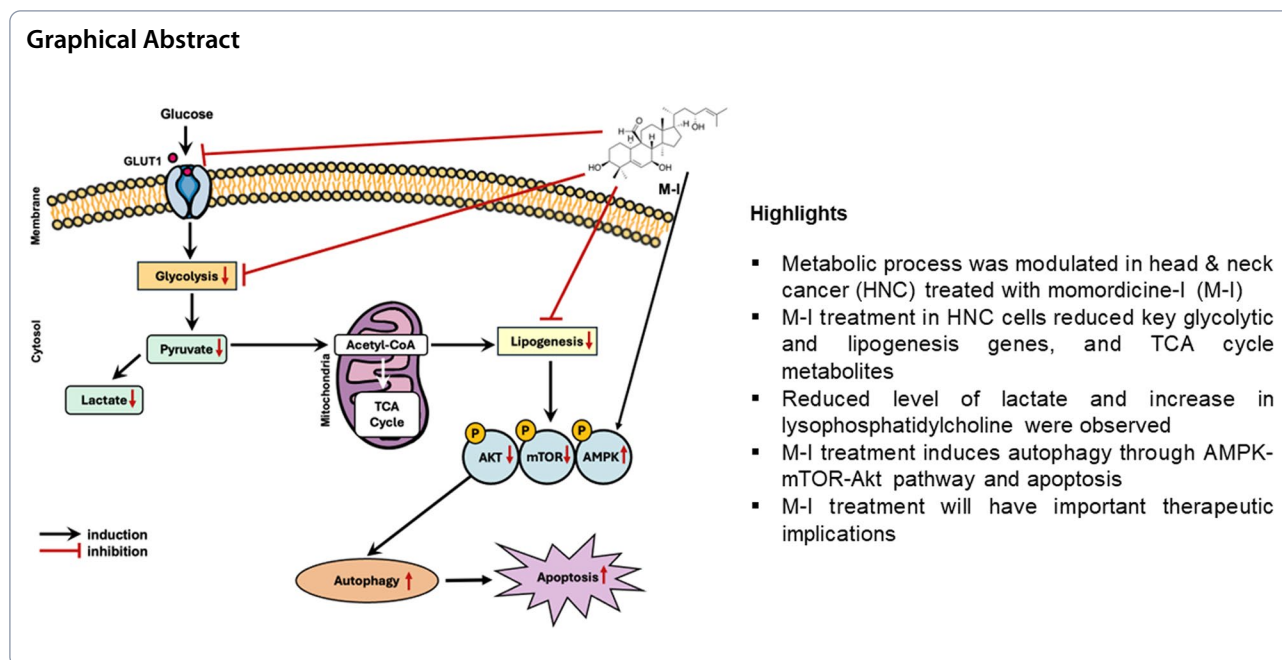
Ratna B. Ray

ratna.ray@health.slu.edu

Full list of author information is available at the end of the article



© The Author(s) 2024. **Open Access** This article is licensed under a Creative Commons Attribution-NonCommercial-NoDerivatives 4.0 International License, which permits any non-commercial use, sharing, distribution and reproduction in any medium or format, as long as you give appropriate credit to the original author(s) and the source, provide a link to the Creative Commons licence, and indicate if you modified the licensed material. You do not have permission under this licence to share adapted material derived from this article or parts of it. The images or other third party material in this article are included in the article's Creative Commons licence, unless indicated otherwise in a credit line to the material. If material is not included in the article's Creative Commons licence and your intended use is not permitted by statutory regulation or exceeds the permitted use, you will need to obtain permission directly from the copyright holder. To view a copy of this licence, visit <http://creativecommons.org/licenses/by-nc-nd/4.0/>.



Introduction

The risk factors for squamous cell carcinoma of the head and neck (HNC), especially oral, pharyngeal and laryngeal cancer, include tobacco use, excessive alcohol consumption, betel quid chewing and human papillomavirus infection. In 2024, an estimated 58,450 new cases of HNC will be diagnosed in the United States and 12,230 people will die from the disease (NCI-Cancer Stat Fact Sheets). Breakthroughs have been elusive due to significant limitations in our understanding of HNC's unique biology. Chemotherapeutic and immunotherapeutic drugs as well as the deployment of radiation therapy have patently improved cancer treatment outcomes, yet significant side effects and the development of drug resistance may be obstacles to cancer treatment. There is a critical need to identify additional therapeutic strategies for successful management of these patients and to understand the basic mechanism of the disease development and progression.

Metabolic reprogramming is one of the hallmarks in cancer progression. Cancer cells display different metabolic profiles than normal cells due to aerobic glycolysis (Warburg effect) and lipogenesis for cancer progression. Alteration in multiple regulatory genes of the glycolysis pathway facilitates abnormal induction of glycolysis in tumorigenesis. Increased glycolysis leads to elevated lactic acid accumulation in the tumor microenvironment which contributes to immune suppression and drug resistance [1]. One important metabolic adaptation in cancer cells is dysregulated glucose metabolism, particularly the increase of glycolysis, which supplies energy and

the precursors for biosynthesis needed for rapid cell division [2]. The glycolytic pathway, encompassing enzymes such as hexokinase (HK), phosphofruktokinase (PFK), and pyruvate dehydrogenase kinase (PDK), is tightly regulated to sustain the high energy demands of cancer cells. Glucose transporter 1 (GLUT1), which promotes glucose absorption into cells, and lactate dehydrogenase A (LDHA) which converts pyruvate to lactate, are characteristic of aerobic glycolysis in cancer cells, and two important regulators of glucose metabolism. Dysregulated expression of these glycolytic genes is common in HNC and other malignancies, which promotes tumor growth. However, inhibitors of HK, PDK or LDHA have limited efficacy in vivo due to toxicity or non-specific effect [3, 4].

Excess pyruvate can facilitate either mitochondrial TCA cycle and electron transport chain activity or biosynthetic pathways such as de novo lipogenesis. Cancer cells can enhance lipogenesis and fatty acid oxidation for energy production, maintaining membrane integrity, preventing ROS and stress induced damage [5]. Like glycolysis, alterations in lipid metabolism, particularly de novo lipogenesis, or the synthesis of lipids from alternative carbon sources plays a pivotal role in cancer cell survival and growth [6]. This biosynthesis of fatty acids and phospholipid/neutral lipids, regulated by enzymes such as ATP-citrate lyase (ACLY), acetyl-CoA carboxylase (ACC), and fatty acid synthase (FASN), supports both lipid oxidative metabolism, membrane biogenesis/maintenance, and signaling pathways vital

for cancer cell proliferation. Therefore, targeting these pathways may have a broad range of implications in controlling cancers [7].

Natural products have anti-cancer properties, particularly in the regulation of glycolysis and lipid metabolism, and the activation of cell death [8–10]. Active ingredients derived from natural products are drawing attention as an alternative approach for anti-cancer therapy [6]. The utilization of phytochemicals with potential pharmacological effects is one of the emerging strategies [11]. Momordicine-I (M-I), a bioactive compound derived from *Momordica charantia* (bitter melon), has emerged as a potential therapeutic agent in cancer due to its multifaceted effects on cellular processes [12–14]. In this study, we observed that M-I treatment of HNC cells inhibits glycolysis and lipogenesis signaling and induces autophagy. To the best of our knowledge, this is the first study describing the metabolic modulation by M-I in HNC cancer cells.

Methods

Cell culture

HNC cell lines Cal27 and JHU22 were cultured in Dulbecco's Modified Eagle's Medium (DMEM) [14] supplemented with 10% fetal bovine serum (FBS) and 1% penicillin–streptomycin at 37 °C in a humidified atmosphere with 5% CO₂. The mouse oral squamous cell carcinoma (MOC2) cell line was cultured in RPMI 1640 medium supplemented with 10% FBS and 1% penicillin–streptomycin [14].

Momordicine-I preparation and treatment

The momordicine-I (>98% pure) was purchased from Chemfaces (Cat. No.: CFN92076; Hubei, China). The powder was dissolved in DMSO, and cells treated at concentrations as stated in figure legends. Based on cytotoxicity data, unless otherwise specified Cal27 and JHU22 cells were treated with 10 µg/mL and 15 µg/mL dose of M-I, respectively. Diluted DMSO (vehicle) was used as control and referred as Con. All the experiments were performed at least in triplicate.

RNA isolation and quantitative real-time PCR

Total RNA was isolated using TRIzol reagent (Invitrogen, CA). cDNA was synthesized using a random hexamer with Superscript III reverse transcriptase (Thermo Fisher Scientific). The qRT-PCR was performed for quantitation of gene expression using specific primers (Table 1) by SYBR green based detection system (Thermo Fisher Scientific) as per standard procedure. 18 s rRNA was used as endogenous control gene CT value, and relative gene expression was measured using the $2^{-\Delta\Delta CT}$ formula

($\Delta\Delta CT = \Delta CT$ of the sample – ΔCT of the untreated control). Each sample was loaded in triplicate.

Western blotting

Cell lysates were prepared using 2X SDS sample buffer, and western blot analysis was performed using specific antibodies to GLUT-1 (1: 1000, Cell Signaling Technology, CST), LDHA (1:1000, SantaCruz), ACLY (1:1000, Cell Signaling Technology, CST), p62 and FASN (1:1000, SantaCruz), Cleaved PARP, LC3, AMPK, pAMPK, mTOT, pmTOR, Akt, and pAkt (1:1000, CST). The HRP-conjugated anti mouse or anti-rabbit secondary antibodies (1:2000) were purchased from Santa Cruz Biotechnology (SBT). The membrane was re probed with Actin-HRP antibody (1:2500, SBT) or tubulin antibody (1:1000, SBT) to compare protein loading in each lane.

Shotgun lipidomics of phosphatidylcholine and lysophosphatidylcholine molecular species

Lipids were extracted from control or M-I treated oral cancer cells as described previously [4]. Briefly, cell suspensions were subsequently subjected to modified Bligh-Dyer extraction in the presence of lipid class internal standards, 1-heptadecanoyl-sn-glycero-3-phosphocholine and 1,2-dieicosanoyl-sn-glycero-3-phosphocholine. For phospholipids, lipid extracts were diluted in methanol/chloroform (4/1, v/v), and molecular species were quantified by electrospray ionization-tandem mass spectrometry (ESI-MS/MS) on a triple quadrupole mass spectrometry instrument using shotgun lipidomics. Phosphatidylcholine molecular species were quantified as chlorinated adducts in the negative-ion mode using neutral loss scanning for 50 amu (collision energy = 24 eV). Lysophosphatidylcholine molecular species were quantified as sodiated adducts in the positive-ion mode using neutral loss scanning for 59.1 amu (collision energy = –28 eV). Individual molecular species were quantified by comparing the ion intensities of the individual molecular species to that of the lipid class internal standard, with additional corrections for type I and type II [13C] isotope effects.

Lactate production and mitochondrial membrane potential assay

To measure the lactate production, glycolysis kit (Dojindo Laboratories-G272) was used according to the instruction. Lactate working solution was added to the culture supernatants, incubated at 37 °C for 30 min, and measured the absorbance at 450 nm. Mitochondrial membrane potential was assessed using the JC-1 MitoMP Detection Kit (Dojindo Laboratories)

Table 1 List of primes used in qRT-PCR

Gene	Species	Primer type	Sequence
GLUT1	Hs	FP	5'-GGGGTCTATAAACGCTACGG-3'
		RP	5'-GGGGGCATTGATGACTCCAG-3'
FASN	Hs	FP	5'-GCAAGCTGAAGGACCTGTCT-3'
		RP	5'-TCCTCGGAGTGAATCTGGGT-3'
FASN	Mm	FP	5'-GATGGAAGGCTGGCTCTATG-3'
		RP	5'-GTTTCGTTCTCGGAGTGAGG-3'
PKM	Hs	FP	5'-CAGAGGCTGCCATCTACCAC-3'
		RP	5'-GGCCTTGCCAACATTCATGG-3'
PDK3	Mm	FP	5'-ACACTAACCTGCACATCCG-3'
		RP	5'-GAATGGGTTTGTGGCGCT-3'
PDK3	Hs	FP	5'-CCCCTTTGGCTGGATTGGTTA-3'
		RP	5'-CACAGAGAGACCACAGCATT-3'
LDHA	Hs	FP	5'-AGCTGTTCCACTTAAGGCC-3'
		RP	5'-TGGAAACAAAAGGAATCGGGA-3'
LDHA	Mm	FP	5'-CCTTCTCGTCTGAGCTGTGG-3'
		RP	5'-CAGGCTCACAGGGTAATCG-3'
ACLY	Hs	FP	5'-GACTTCGGCAGAGGTAGAGC-3'
		RP	5'-TCAGGAGTGACCCGAGCATA-3'
SREBP-1C	Hs	FP	5'-TTTGAGGACAGCAAGACAGAAT-3'
		RP	5'-ATTGAGCAGCCAGACCACTG-3'
Srebf1	Mm	FP	5'-GAACAGACTGGCCGAGAT-3'
		RP	5'-CTCAGGAGAGTTGGCACCTG-3'
HK1	Hs	FP	5'-AGTTTGACAGGGAGATAGACC-3'
		RP	5'-CATCACTGGTGTAAACTTCC-3'
HK1	Mm	FP	5'-ATTGTAGCTGGTGAATGAC-3'
		RP	5'-TCAAACCTGTTCGAATGTCT-3'
PFKP	Hs	FP	5'-CAGAAGTACGCCTACCTCAAC-3'
		RP	5'-CTCCAGAACGAAGTCTCTCT-3'
ACC1	Hs	FP	5'-TCACACCTGAAGACCTTAAAGCC-3'
		RP	5'-AGCCACACTGCTGTACTG-3'
ACC1	Mm	FP	5'-AGGCGGATATCTGCTGAGAC-3'
		RP	5'-ATCGGGAGTGCTGGTTTAGC-3'
SCD1	Hs	FP	5'-GGAGCTCATCGTCTGTGGAG-3'
		RP	5'-GCCAGTTTGTAGTACCTCT-3'

according to the manufacturer's instructions. Briefly, treated and untreated cells were incubated with JC-1 dye for 30 min at 37 °C. After washing, fluorescence was measured using a microplate reader, with JC-1 monomers (green fluorescence) indicating depolarized mitochondria and J-aggregates (red fluorescence) indicating polarized mitochondria.

Oxygen Consumption Rate (OCR) measurement

OCR was measured using a Seahorse XFe96 Extracellular Flux Analyzer (Agilent Technologies) to assess

cellular respiration in Cal27 and JHU22 cells. The cells were seeded in XFe96 microplates at a density of 15,000 cells for Cal27 or 20,000 cells for JHU22 per well and treated with M-I for 24 h. Culture medium was replaced with Seahorse DMEM medium supplemented with 1 mM pyruvate, 2 mM glutamine, and 10 mM glucose, and the cells were incubated in a non-CO₂ incubator at 37 °C for 1 h. Baseline OCR measurements were taken, followed by the sequential addition of mitochondrial stress agents using the Seahorse XF Cell Mito Stress Test Kit: Oligomycin (1.5 μM): inhibits ATP synthase to measure ATP-linked respiration. FCCP (1 μM): uncouples the mitochondrial membrane, allowing for the measurement of maximal respiration. Rotenone (0.5 μM) and Antimycin A (0.5 μM): inhibit complex I and III of the electron transport chain, respectively, to determine non-mitochondrial respiration. Three measurements were recorded in each condition. After averaging these three timepoints, further calculations were made. Basal respiration rates were calculated as the baseline rates minus the non-mitochondrial respiration rates. ATP-linked respiration rates were calculated as the baseline rates minus the oligomycin-treated respiration rates. And maximal respiration rates were calculated as the FCCP-induced respiration rates minus the non-mitochondrial respiration rates.

BODIPY lipid staining

HNC cells were stained by boron-dipyrromethene (BODIPY) 493/503 (Invitrogen) for 1 h and observed lipid accumulation. Stained cells were visualized with Leica fluorescence microscope in 20X.

Metabolomics analysis

Metabolites were extracted from treated and untreated cells (in two time points) using ice-cold methanol. Metabolite extracts were subjected to liquid chromatography-mass spectrometry (LC-MS) analysis at the Center of Mass Spectrometry and Metabolic Tracing (Washington University). Briefly, ultra-high performance liquid chromatography coupled with mass spectrometry (UHPLC/MS) analyses were conducted using a Thermo Scientific Vanquish Flex UHPLC system, interfaced with a Thermo Scientific Orbitrap ID-X Tribrid Mass Spectrometer. For the separation of polar metabolites, a HILICON iHILIC-(P) Classic HILIC column (100×2.1 mm, 5 μm) with a HILICON iHILIC-(P) Classic guard column (20×2.1 mm, 5 μm) was utilized. The mobile-phase solvents consisted of solvent A=20 mM ammonium bicarbonate, 2.5 μM medronic acid, 0.1% ammonium hydroxide in 95:5 water:acetonitrile and solvent B=95:5

acetonitrile:water. The column compartment temperature was maintained at 45 °C, and metabolites were eluted using a linear gradient at a flow rate of 0.25 mL/min as follows: 0–1 min, 90% B; 12 min, 35% B; 12.5–14.5 min, 25% B; 15 min, back to 90% B. The injection volume was 2 µL. Data was acquired in both positive and negative ion modes. The LC/MS data were then processed and analyzed using Skyline [15] by comparing retention times and mass spectra to standard compounds or metabolite databases.

Tumorigenicity assay

MOC2 cells (1×10^6) containing 40% Matrigel were injected subcutaneously into the flank of C57BL/6 mice (6–7 weeks old), purchased from Charles River. Mice ($n=5$) were randomly divided into two groups when palpable tumors developed (>80 – 100 mm³). The treatment group received 30 mg/kg/mouse of M-I (100 µL M-I was dissolved in 5% DMSO/95% of a 30% w:v Captisol solution) intraperitoneally once daily, and the control group received equal volume of vehicle solution, as described previously [12]. Body weight was monitored, tumor size was measured using a slide caliper, and tumor volume was calculated using the formula $\frac{1}{2} L \times W^2$. At the end-point, mice were euthanized humanely, and tumors were collected for mRNA analysis. All animal experiments were performed in accordance with NIH guidelines following a protocol approved (protocol # 1017) by the Institutional Animal Care and Use Committee (IACUC) of Saint Louis University.

Statistical analysis

Results are presented as mean \pm standard deviation (SD). Statistical significance was determined using Student's t-test or one-way ANOVA. Data were analysed using GraphPad Prism software. A p -value < 0.05 was considered statistically significant. All experiments were repeated at least three times, and representative data are shown.

Results

Momordicine I (M-I) treatment modulates glycolytic gene expression

Glucose metabolism is markedly altered during proliferation and is a key feature of cancer cell metabolism. In the glycolytic pathway, hexokinase (HK) catalyses the first committed step in glucose metabolism by phosphorylating glucose to produce glucose-6-phosphate. GLUT1, a membrane protein, is the limiting step in the glucose flux into metabolic pathways [16]. GLUT-1 is

highly expressed in several cancers including head and neck cancer [17]. To investigate whether M-I exerts an effect on glucose metabolism in HNC cells, we treated the Cal27 and JHU22 cells with M-I for 30 h and analysed changes in glycolysis genes. A significant downregulation of *HK1* and *SLC2A1* (GLUT-1) expression was observed in both the cell lines following M-I treatment (Fig. 1). Phosphofructokinase (PFK) catalyses another key regulatory step that converts fructose 6-phosphate to fructose 1, 6-bisphosphate, and *PFKP* is a major isoform of cancer cells. In oral cancer, regulation of *PFKP* expression promotes cell proliferation, migration, and invasion [18]. *PFKP* mRNA was also decreased in both cells following M-I treatment (Fig. 1).

Pyruvate kinase converts phosphoenolpyruvate to pyruvate and ADP. PKM is known to be involved in progression of cell proliferation and migration and inhibiting apoptosis in HNC [19, 20]. M-I reduced *PKM* expression in both HNC cell lines (Fig. 1). Pyruvate dehydrogenase kinase (PDK) regulates the activity of pyruvate dehydrogenase (PDH) by phosphorylation. Phosphorylated PDH is inactivated, thus reducing the conversion of pyruvate to acetyl-CoA. We observed decreased *PDK3* mRNA in HNC cells following M-I treatment (Fig. 1). Altogether, these expression changes suggest that M-I decreases glycolytic and oxidative glucose metabolism in HNC cells. To further investigate the metabolic impact of M-I on HNC cells, we conducted a comprehensive metabolomics study. Our study revealed significant alterations in the metabolic profile of HNC cells following treatment with M-I.

Lactate dehydrogenase-A (LDHA) facilitates glycolysis by converting pyruvate to lactate and replenishing NAD⁺. Lactate is produced in significant quantities in cancer cells. It causes the extracellular pH in the tumor microenvironment to become more acidic which promotes metastasis, angiogenesis, and immunosuppression. In Cal27 and JHU22 cells, *LDHA* mRNA expression was significantly downregulated in M-I treated groups as compared to respective control groups (Fig. 1). Next, we measured the total lactate levels in Cal27 and JHU22 cells and observed significantly lower levels of lactate production in M-I treated cells (Fig. 2A). We also observed inhibition of GLUT1 and LDHA protein expression following M-I treatment in both cell lines (Fig. 2B). Furthermore, we also investigated the effect M-I treatment on glycolytic gene expression in mouse oral squamous cell carcinoma (MOC2) cells. Similarly to the human cell lines, M-I reduced expression of *Hk1*, *Pdk3*, and *Ldha* (Fig. 2C), further suggesting a reduction in glycolytic metabolism by M-I treatment.

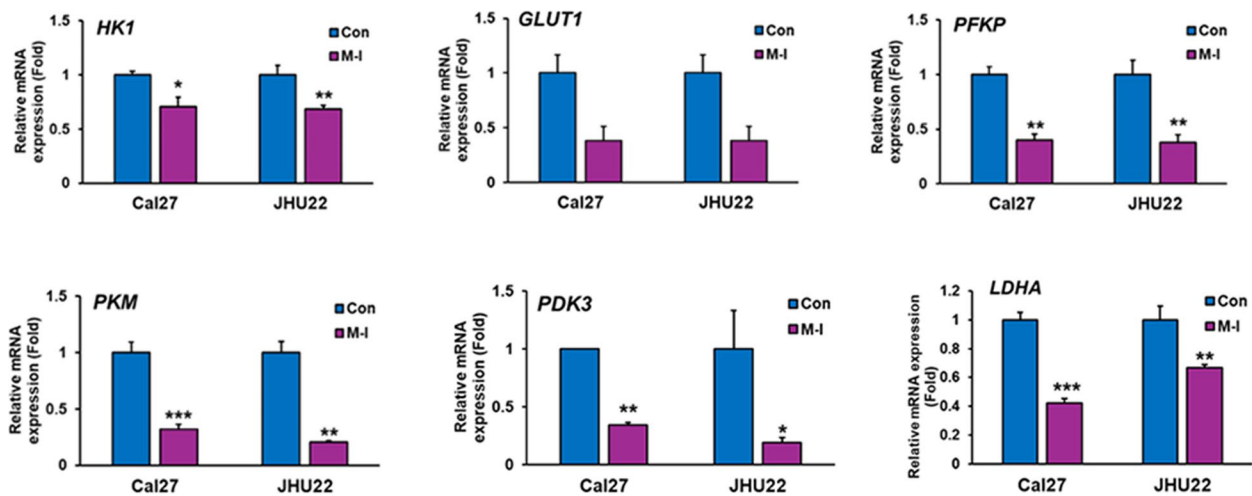


Fig. 1 M-I treatment decreases expression of glycolytic genes in HNC cells. Relative mRNA expression of *HK1*, *GLUT-1*, *PFKP*, *PKM*, *PDK3*, and *LDHA* was analysed by q-RT-PCR in Cal27 and JHU22 cells with or without M-I treatment. Vehicle (DMSO) was used as control (Con). 18 s gene was used as internal control. Data were analysed by Student's t-test. Small bars indicate standard error (* $P < 0.05$, ** $P < 0.01$; *** $P < 0.001$). $n = 3$ biological replicates and 3 technical replicates

M-I alters metabolite pool size in HNC cells

The lactate production was significantly decreased in cells treated with M-I, confirming that glycolysis was suppressed. We further performed metabolomic study using Cal 27 cells treated with M-I for (10 h-M-I-1 and

22 h (M-I-2). Metabolites associated with the glycolytic pathway were markedly reduced in M-I-treated cells compared to controls. The pool size of several intermediates of the TCA cycle (malate, citrate, isocitrate, alpha-ketoglutarate) were reduced in Cal27 cells following

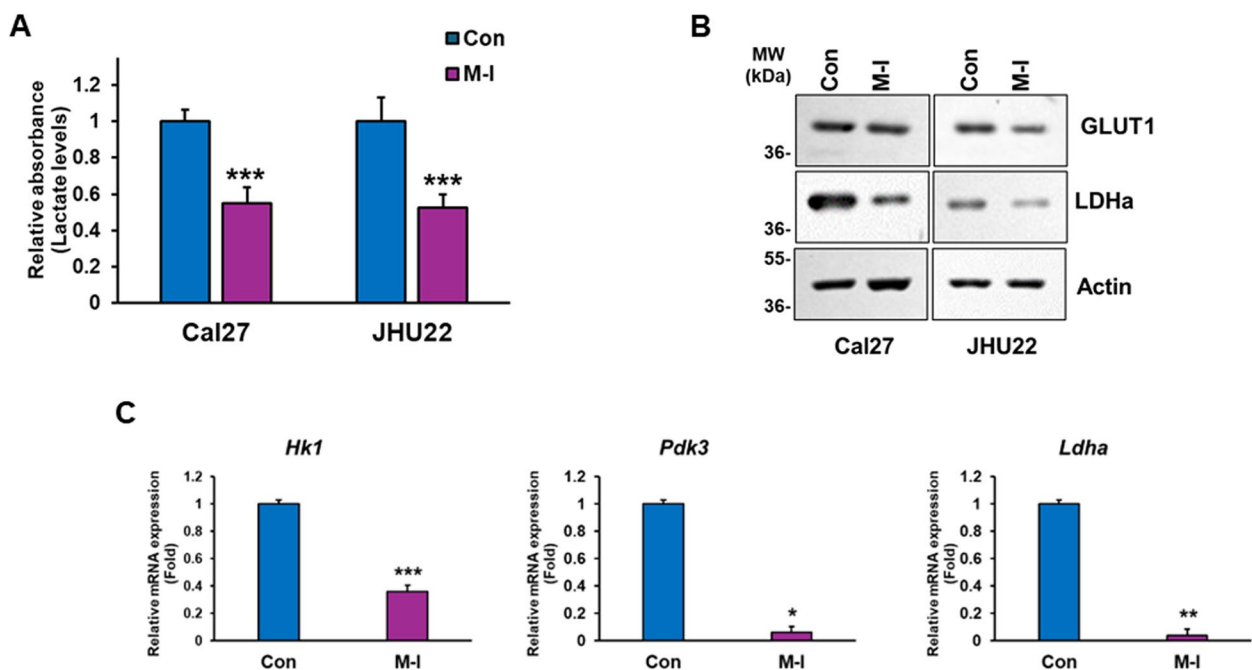


Fig. 2 M-I inhibits lactate production in HNC cells. **A** Cal27 and JHU22 cells were treated with M-I for 30 h and analysed for lactate production at 450 nm. Data were analysed by Student's t-test. Small bars indicate standard error (*** $P < 0.001$). $n = 3$ biological replicates. **B** Lysates from Cal27 and JHU22 cells treated with M-I were analysed for GLUT1 or LDHa expression by western blot using specific antibody. The blot was reprobbed with Actin antibody as an internal control. **C** Mouse oral cancer (MOC2) cells were treated with M-I. Total RNA was isolated from ~30 h of treatment and expression of glycolytic genes (*Hk1*, *Pdk3* and *Ldha*) was measured by qRT-PCR. 18 s gene was used as internal control. Data were analysed by Student's t-test. Small bars indicate standard error (* $P < 0.05$, ** $P < 0.01$; *** $P < 0.001$). $n = 3$ biological replicates and 3 technical replicates

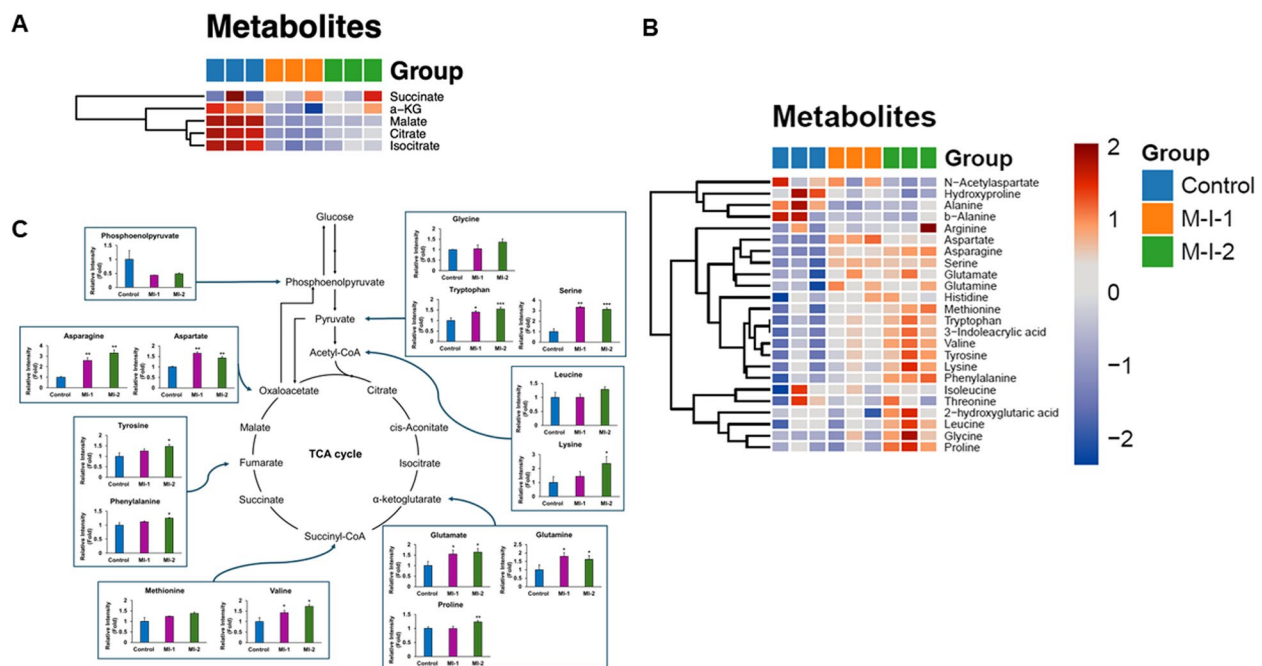


Fig. 3 M-I alters metabolites in TCA cycles and amino acids. **A** M-I inhibit TCA intermediates following 10 h (M-I-1) and 22 h (M-I-2) of treatment in Cal 27 cells. Blue color in heatmap is untreated control, orange colour is cells treated for 10 h and green colour is cells treated for 22 h. **B-C** M-I treatment enhances amino acids following treatment. $n=3$ biological replicates

M-I treatment (Fig. 3A). On the other hand, the levels of amino acids (arginine, asparagine, glycine, histidine, leucine, lysine, methionine, phenylalanine, proline, serine, threonine, tryptophan, tyrosine, and valine) were increased (Fig. 3B-C), suggesting that cells may exert another energy acquisition for survival or cells are taking up amino acids to compensate for reduced glucose utilization in TCA. These findings suggest that M-I treatment disrupts central metabolic pathways crucial for cancer cell energy production and biosynthesis.

M-I treatment modulates de novo lipogenesis

Cancer cells depend on lipogenesis to fuel membrane growth for proliferation. To begin to investigate whether M-I modulates de novo lipogenesis, we examined the mRNA and protein expression of key enzymes. We observed a significant downregulation of mRNA expression of *ACLY*, *ACCI1*, *FASN* and *SCD1* following M-I treatment in both human HNC cell types (Fig. 4A). These lipogenesis genes are strongly controlled by the transcription factor sterol regulatory element-binding protein (SREBP) and M-I treatment also decreased *SREBP1* expression in Cal27 and JHU22 cells. Additionally, we observed reduced protein levels of *ACLY* and *FASN* in M-I treated groups of Cal27 and JHU22 cells (Fig. 4B). We further observed inhibition of *Fasn*, *Acc1*, and *Srebf1* in M-I treated murine MOC2 cells (Fig. 4C). These gene

expression changes strongly suggest M-I reduces de novo lipogenesis.

To further assess the effect of M-I on lipid content in HNSCC cells, shotgun lipidomics was conducted using Cal27 and JHU22 cell lines following M-I treatment to elucidate alterations in lipid composition. Phospholipid composition provides insight into alterations in cellular membranes, which play vital roles in disease pathways. We observed an enhancement of lysophosphatidylcholine (LPC) following M-I treatment in Cal27 (A) and JHU22 (B) cells accompanied by decreased levels of several phosphatidylcholine (PC) molecular species (Fig. 5).

M-I rewires mitochondrial function

Enhanced LPC may contribute to mitochondrial dysfunction [21]. We next tested the mitochondrial membrane potential by a JC-1 assay which showed reduced mitochondrial membrane potential in HNC cells with M-I treatment (Fig. 5C). Mitochondria are key players in regulation of cellular bioenergetics and produce the bulk of adenosine triphosphate by oxidative phosphorylation (OXPHOS). Cancer cells actively use anaerobic glycolysis or combination of OXPHOS and glycolysis for ATP production under stress for survival. To test whether M-I affects the OXPHOS

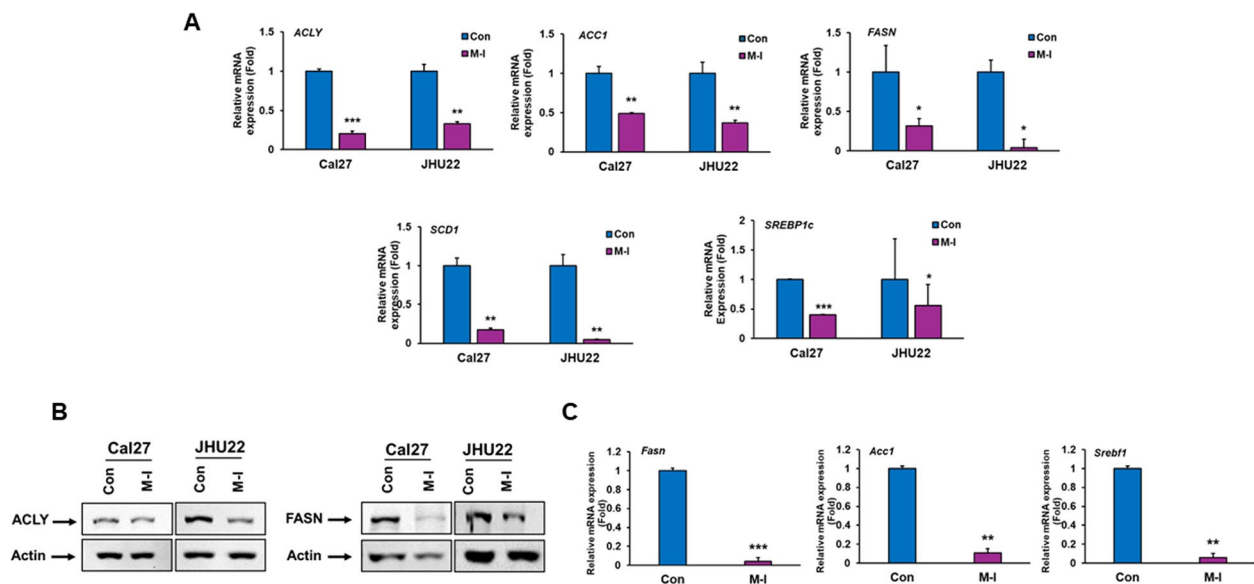


Fig. 4 M-I treatment inhibits expression of different enzymes of de novo lipogenesis in HNC cells. **A** Relative mRNA expression of *ACLY*, *ACC1*, *FASN*, *SCD1* and *SREBP1c* was analysed by qRT-PCR in Cal27 and JHU22 cells with or without M-I treatment. Vehicle was used as control (Con). 18 s gene was used as internal control. Small bar indicates standard error (* $P < 0.05$, ** $P < 0.01$; *** $P < 0.001$). $n = 3$ biological replicates and 3 technical replicates. **B** Lysates from Cal27 and JHU22 cells treated with M-I were subjected to western blot analysis for *ACLY* and *FASN* using specific antibodies. The membrane was reprobbed with antibody to actin as an internal control. **C** Total RNA was isolated from MOC2 cells treated with M-I, and expression of *Fasn*, *Acc1* and *Srebf1* was measured by qRT-PCR. 18 s gene was used as internal control. Data were analysed by Student's t-test. Small bars indicate standard error (* $P < 0.05$, ** $P < 0.01$; *** $P < 0.001$). $n = 3$ biological replicates and 2 technical replicates

capacity of HNC cells, we measured the oxygen consumption rates (OCR) of HNC cells with and without M-I treatment by the Seahorse bioanalyzer. A significant decrease in these parameters were observed in Cal27 (D) and JHU22 cells (E) following M-I treatment (Fig. 5).

M-I induces autophagy in HNC cells

To test the lipid accumulation following M-I treatment, cells were stained with lipophilic dye BODIPY 493/503. Interestingly, we noted distinct punctate dots in M-I treated JHU22 cells (Fig. 6A), suggesting induction of autophagy. Autophagy is emerging as a double-edged sword in cancer and is highly context-specific depending on the cell type, tumor microenvironment, disease stage, and external stimuli. To further validate, we examined the effect of M-I treatment on formation of the autophagosome membrane by detecting the conversion of LC3I to lipidated LC3II. M-I treatment in JHU22 cells triggered autophagy as compared to control cells, as indicated by increased LC3II (Fig. 6B, left panel), corroborating the appearance of punctate dots observed in BODIPY staining. Autophagic flux is defined as a measure of autophagic degradation activity [22]. LC3-II level is an indicative of autophagic flux and we observed much higher LC3II level in M-I treated cells. The p62 levels are negatively correlated

with autophagic flux. We examined the expression level of p62 by Western blot analysis and interestingly observed that accumulation of p62 expression in M-I treated cells (Fig. 6B, right panel). p62 accumulation is correlated with apoptotic cell death [23]. We showed that bitter melon treatment accumulates p62 expression breast cancer cells [24]. The PI3K/AKT/mammalian target of rapamycin (mTOR)/p70S6K pathways are frequently amplified in oral cancer [24, 25]. Modulation of the AMPK/mTOR pathway is also associated with the initiating of autophagy in cancer cells. To investigate whether the AMPK/mTOR pathway was involved in M-I-induced autophagy, we observed that M-I activates pAMPK^{T172} and reduces pmTOR^{S2448} in JHU22 cells (Fig. 6C). The higher total mTOR expression in M-I treated samples is most likely due to inhibition of mTOR phosphorylation. Inhibition of pAkt^{T308} in JHU22 cell lines following M-I treatment was observed (Fig. 6C). To investigate whether induction of autophagy is related to lipogenesis, we treated the cells with Bafilomycin A1, an inhibitor of autophagosome-lysosome fusion, along with M-I. We measured mRNA expression of *FASN*, *ACC1* and *ACLY* in M-I or M-I + Baf1 treated cells. Our results suggested that blocking autophagy does not rescue the M-I mediated decrease in expression of lipogenesis genes (Fig. 6D). Together, our results showed that AMPK/mTOR/Akt

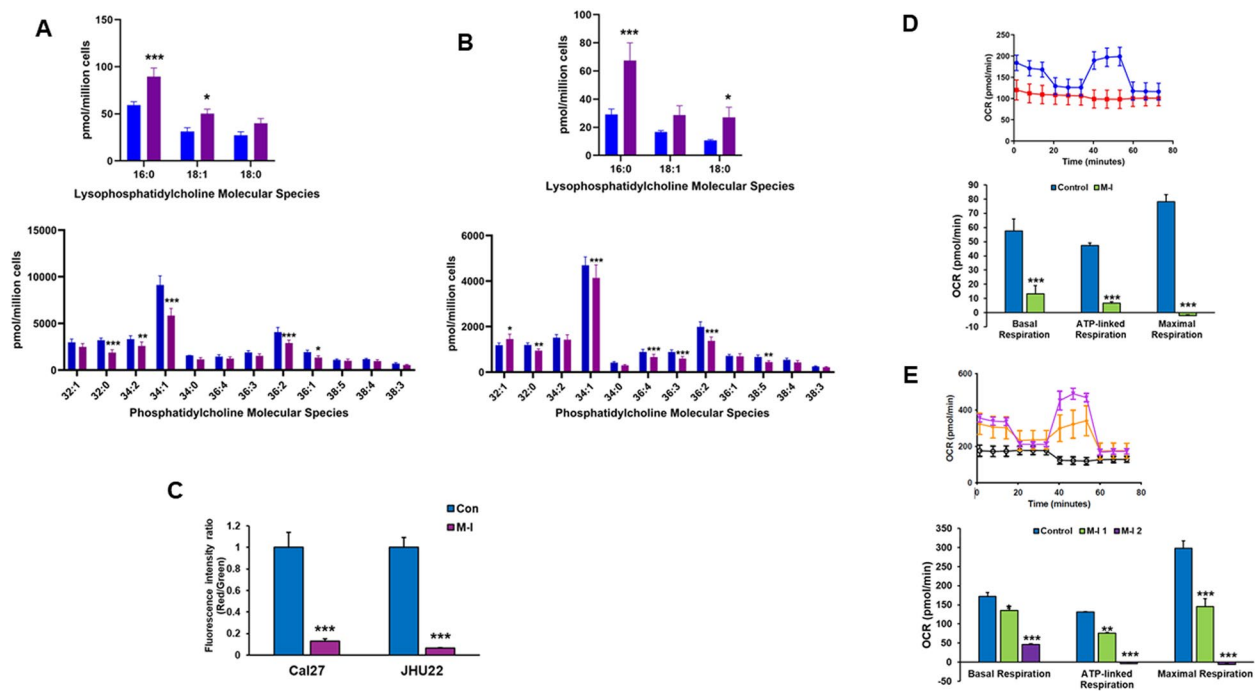


Fig. 5 HNC cells treated with M-I enhances lysophosphatidylcholine (LPC) levels. Cal27 (A) and JHU22 (B) cells were treated with M-I and lipid profile was analysed by electrospray ionization-tandem mass spectrometry (ESI-MS/MS), respectively. Representative mass-spectra showing lysophosphatidylcholine (top panel) and phosphatidylcholine (bottom panel). C M-I treatment reduces mitochondrial membrane potential in Cal27 and JHU22 cells as measured by JC-1 activity. (* $P < 0.05$, ** $P < 0.01$, *** $P < 0.001$). $n = 2$ biological replicates and 3 technical replicates. D, E Oxygen consumption rate (OCR) was assessed using the Seahorse XF extracellular flux analyser. Cal27 cells (D) were treated with M-I (5 ug/ml) for 24 h. JHU22 cells (E) were treated with M-I (10 ug/ml -orange, 15ug/ml-black) for 24 h. Data are plotted to demonstrate the differences in the basal respiration rate, ATP-linked respiration, and maximal respiratory capacity (bottom panels). Small bars indicate standard error (* $P < 0.05$, ** $P < 0.001$). $n = 2$ biological replicates and 10 technical replicates

signaling pathway plays a crucial role in M-I-induced autophagy in HNC cells. LC3 can serve as a platform to facilitate apoptosis [26]. We further observed PARP cleavage in M-I treated JHU22 cells (Fig. 6E). In-depth mechanism of how autophagy leads to apoptosis in M-I treated HNC cells needs further investigation.

M-I treatment represses metabolic pathway in vivo

To investigate whether M-I treatment alters the metabolic pathways genes in mouse oral cancer, we generated tumors in C57BL/6 mice by implanting murine MOC2 cells as described previously [14]. As expected, M-I treatment significantly inhibited tumor growth without altering body weight (Fig. 7A-B). Expression of glycolytic enzymes *Hk1* and *Pdk3*, and lipogenic enzymes *Fasn* and *Acly* were tested from these tumors and M-I treatment induced a significant decrease in both genes (Fig. 7C), in agreement with in vitro results. We reported previously that M-I treatment does not alter blood glucose level in tumor bearing mice [12].

Discussion

Cancer cell metabolic pathways are reprogrammed during tumor progression. In this study, we showed that M-I modulates glucose and lipid metabolism and induces autophagy in HNC cells. The metabolic reprogramming is facilitated by M-I through inhibition of (i) crucial regulatory genes (GLUT1, PKM, PDK3) of the glycolysis pathway resulting in reduction in lactate production, (ii) inhibition of key fatty acid synthesis genes (ACLY, ACC1, FASN), leading to an increase of lysophosphatidylcholine and mitochondrial dysfunction, and (iii) induction of autophagy. We further observed reduced expression glycolytic and lipogenesis molecules M-I treated HNC mouse tumors.

Glucose is an important source of energy and carbon in normal and cancer cells. GLUT1, a key glucose transporter, often overexpresses in cancers and facilitates increased glucose uptake to support the metabolic demands of dividing cancer cells [27, 28]. The substantial reduction in GLUT 1 expression following M-I treatment suggests that M-I disrupts the metabolic balance of HNC cells. Overexpression of PFKP and PKM2 was reported

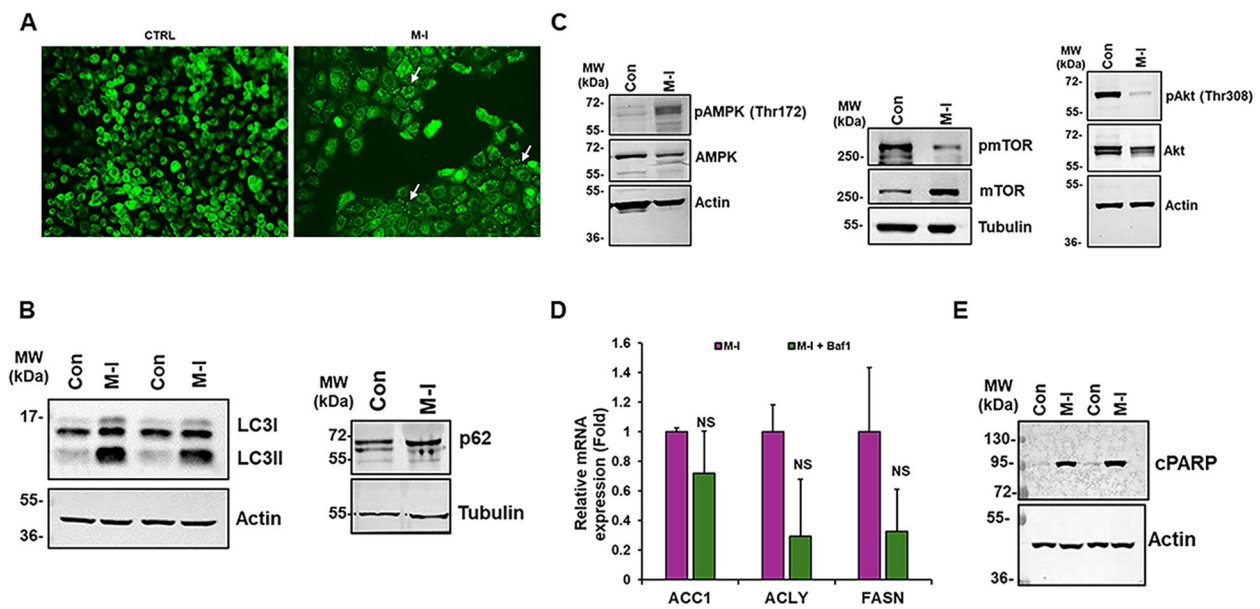


Fig. 6 M-I treatment induces autophagy in HNC cells. **A** M-I treated JHU22 cells were stained with BODIPY (green). A representative image (20×) is shown. White arrows indicate the puncta dots. **B** Cell lysates were analysed by western blot for LC3 (16 kDa and 14 kDa) expression using specific antibody (left panel). Cell lysates were analysed by Western blot for p62 (62kDa) expression using specific antibody (right panel). The blot was reprobbed with an antibody to actin or tubulin for comparison of protein load. **C** JHU22 Cell lysates were analysed by western blot for pAMPK^{T172}/AMPK (62 kDa), p-mTOR^{S2448}/mTOR (289 kDa) and pAkt^{T308}/Akt (60kDa) expression using specific antibodies. The blots were reprobbed with an antibody to actin for comparison of protein load. **D** M-I treated HNC cells were treatment with Bafilomycin A1, an inhibitor of autophagosome-lysosome fusion. Relative mRNA expression of *ACC1*, *ACLY* and *FASN* was analysed by qRT-PCR and normalized by 18 s RNA. *n* = 2 biological replicates and 2 technical replicates. **E** JHU22 cell lysates were analysed by Western blot for cleaved PARP (cPARP) expression using specific antibody. The blot was reprobbed with an antibody to actin for comparison of protein load

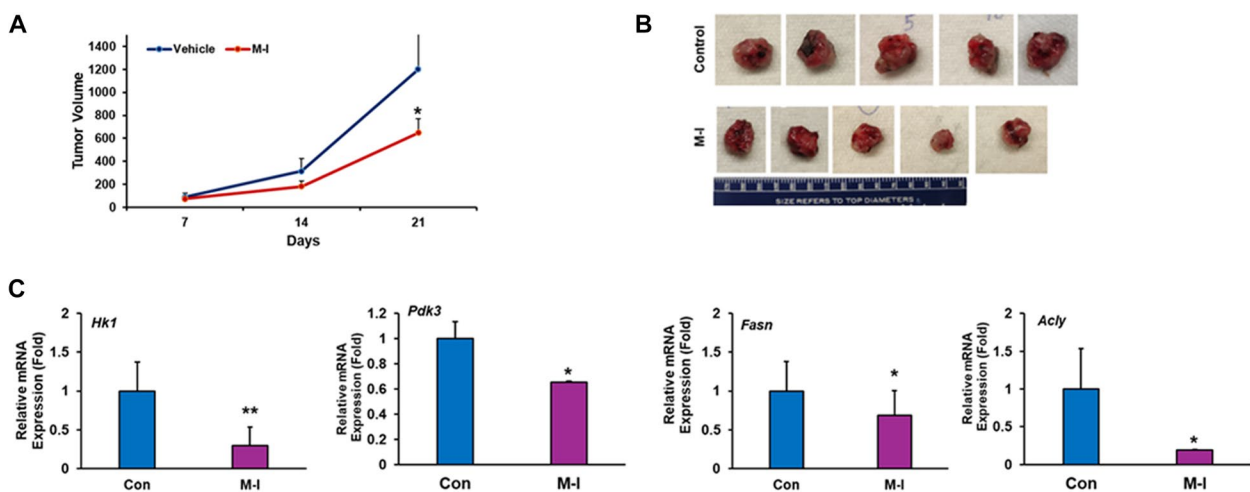


Fig. 7 M-I treatment inhibits glycolysis and lipogenesis in vivo. MOC2 cells (1×10^6) were injected subcutaneously into C57BL/6 mice. Tumor-bearing mice were randomly divided into two groups. The control group received vehicle, and the experimental group received 30 mg/kg/mouse M-I via intraperitoneal injection every day until the end of the experiment. **A** Tumor volume post-M-I treatment. **B** Representative images of tumors from control and M-I-treated groups. **C** Relative mRNA expression of *Hk1*, *Pdk3*, *Fasn* and *Acty* was analysed by qRT-PCR from control or M-I treated tumor RNA. 18 s gene was used as internal control. Small bar indicates standard error (*, $p < 0.05$; **, $p < 0.01$). *n* = 3 technical replicates

in several cancers including oral cancer and inhibiting these molecules suppress cell growth [4, 29]. Another important glycolytic gene, LDHA, is upregulated in many cancers including HNC. Upregulation of pyruvate dehydrogenase kinase (PDK) isoforms including PDK3 was reported in different cancers and associated with chemoresistance. The reduced expression of HK1, PFKP, PDK3, PKM and LDHA in HNC cells was observed following M-I treatment. M-I may increase pyruvate dehydrogenase activity by suppressing PDK3 hence favoring pyruvate entry into the TCA cycle as opposed to lactate production. Lactate could also be reduced because glucose is being shunted to different pathway. Although targeted therapies for HK, GLUT1 or LDHA have been developed against cancers, the success is limited due to toxicity or non-specific affect. However, we did not observe any systemic toxicity using M-I in this preclinical study and our previous reports [12, 14]. Metabolic reprogramming influences the drug resistance [30]. We and others have shown that bitter melon extracts or M-I inhibited glycolysis in cancer cells [4, 31], however, modulation of glycolysis pathway in non-tumor Hek293 cells following M-I treatment was not noted. Thus, inhibiting several glycolytic genes by M-I in HNC cells suggests its potential therapeutic efficacy.

The de novo lipogenesis is another critical metabolic pathway that enables cancer cells to generate fatty acids from non-lipid precursors, providing a survival advantage by ensuring a continuous supply of lipids for membrane synthesis and energy storage. This multistep process begins with the conversion of cytosolic citrate to acetyl-CoA by ACLY. Acetyl-CoA is then sequentially processed by ACC and FASN to form the saturated fatty acid palmitate. The lipid-modifying enzyme SCD subsequently catalyses the conversion of palmitate to monounsaturated fatty acids, which are further metabolized into various lipid species essential for cellular functions. These enzymes are also important components of the de novo lipogenesis pathway, catalysing consecutive stages in the conversion of citrate to fatty acids, which are essential building blocks for lipid biosynthesis [20, 32]. Elevated expression of SCD1 has been negatively correlated with survival in oral cancer patients underscoring the potential role of de novo lipogenesis in promoting cancer progression [33]. M-I treatment in HNC cells reduced expression of important lipogenic enzymes ACLY, ACC1, FASN, and SCD1, however, no effect on non-tumor Hek293 cells.

Using shotgun lipidomics analysis, we observed enhanced level of LPC in M-I treated HNC cells. PC is one of the most abundant phospholipids in membrane of mammalian cells and subcellular organelles, and cancer cells generally convert free fatty acids for phospholipid

synthesis. The concomitant loss of PC indicates LPC is produced by phospholipase A2 activity or diminished acyltransferase activity in the presence of M-I. LPC increases the production of pro-inflammatory cytokines, induces oxidative stress, and promotes apoptosis [34]. LPC varies greatly among different cancer patients and a lower level of LPC (16:0) has been found in intrahepatic cholangiocarcinoma, ovarian cancer, and colorectal cancer patients. LPC (18:0) inhibits melanoma invasion and metastasis [35]. Enhanced LPC exerts mitochondrial dysfunction. Mitochondria are central to both energy production and apoptotic pathways [36]. The reduction in mitochondrial membrane potential, as indicated by decreased JC-1 activity, suggests that M-I may induce mitochondrial dysfunction. Further, we found that M-I significantly decreased the OCR in HNC cells. Mitochondrial dysfunction can lead to reduced ATP production and increased oxidative stress, potentially triggering cell death pathways [37, 38]. We observed reduced ATP level in our metabolomics study following M-I treatment. Inhibition of glucose and lipid metabolisms induce apoptotic cell death, and we showed induction of apoptosis in M-I treated HNC cells. Further, the concentration of glucose was comparable in M-I treated groups with untreated control mice, with little measurable toxicity.

Lipid metabolic processes have been shown to be involved in the regulation of apoptosis, revealing the role in regulating tumorigenesis [39]. Enhanced glucose uptake is one of the hallmarks of cancer and is regulated by the growth factor signaling pathway that stimulates glucose transporter expression. M-I inhibits GLUT1 expression suggesting that downstream pathways are altered resulting in less energy production. Although amino acids play an important role in cancer metabolism [40], targeting them as a single agent may influence normal cells and may have systemic toxicity. Therefore, key point needs to be considered when targeting the amino acid metabolism, not to generate toxicity in normal tissues, and M-I did not display any noticeable toxicity in the preclinical studies [12, 14].

Autophagy is an evolutionally conserved catabolic process in all eukaryotic cells, however, two opposite mechanisms for autophagy in cancer development have been reported. A growing body of evidence has indicated that several natural products can be an autophagy inducer for an anticancer therapy [24, 41, 42]. We observed M-I treatment induces autophagy in HNC cells independent of modulation of lipogenesis. AMPK, an important sensor of intracellular energy levels, maintains normal energy balance by regulating cellular metabolism and inhibits mTOR signaling pathway for mechanistic modulation of autophagy. Our data demonstrated that the induction of autophagy by M-I in HNC cells is related

to the inhibition of mTOR/Akt signaling. In cancer, Akt signaling is also one of the key regulators of metabolism. The AKT pathway promotes de novo lipid synthesis via transcriptional and post-translational mechanisms [43]. Thus, inhibition of Akt signaling by M-I may alter de novo lipogenesis and autophagy pathways. The metabolic change-induced energy stress may be one of the important reasons for the cell death [44]. Cancer targeting therapy is more precise with less side effects on the normal tissue as compared to traditional therapy, although mechanism of M-I mediated modulatory role in different signaling pathways remains to be elucidated. In silico analysis suggested the interacting sites of few candidate molecules, however, validation of these molecules is needed.

In summary, current clinical outcomes are insufficiently robust, despite the development of various therapies, and new effective approaches are an unmet need. Metabolic rewiring unquestionably affects cancer cell proliferation, and the translation of metabolic reprogramming into clinical care will be beneficial, however, dependency on metabolic pathways is not universal for all cancer types. The metabolic changes in M-I treated HNC cells could affect the tumor microenvironment, influencing interactions with stromal cells and the immune system. The lipidomic alterations induced by M-I treatment in HNC cells, coupled with the observed mitochondrial dysfunction, underscore the potential of M-I as a multifaceted therapeutic agent. These findings open new avenues for the development of targeted therapies that exploit the unique metabolic dependencies of cancer cells. Our study is the first to demonstrate the multifaceted effects of M-I, isolated from *M. charantia* extract, in reprogramming glucose and lipid metabolism, inducing autophagy, disrupting mitochondrial function in HNC cells, and reducing tumor volume, which highlights its potential as a therapeutic agent targeting metabolic vulnerabilities in cancer.

Abbreviations

M-I	Momordicine-I
HNC	Head and neck Cancer
HK1	Hexokinase1
SLC2A1	Solute Carrier Family 2 Member 1
GLUT-1	Glucose transporter protein type 1
PFKP	Phosphofructokinase, Platelet
LDHA	Lactate Dehydrogenase A
PKM	Pyruvate Kinase, Muscle
PDK3	Pyruvate Dehydrogenase Kinase 3
ACLY	ATP Citrate Lyase
ACC1	Acetyl-CoA Carboxylase 1
FASN	Fatty Acid Synthase
PC	Phosphatidylcholine
LPC	Lysophosphatidylcholine
ROS	Reactive oxygen species
pAMPK	Phosphorylated AMP activated protein kinase
AMPK	AMP activated protein kinase
mTOR	Mammalian Target of Rapamycin

pAkt	Phosphorylated protein kinase B
Akt	Protein kinase B
Baf1	Bafilomycin

Acknowledgements

We thank Jane McHowat for critical reading of the manuscript. We thank Robert Steele, Pradeep Bhartiya and Audrey Brecher for their technical assistance in the initial stages of the work.

Authors' contributions

R.B.R. and M.V. conceived and D.B., E.T.T., and R.B.R. designed the research plan; D.B., M.K.L., E.T.T., R.A.P., C.H., L.P.S., G.J.P., D.F., K.M., and R.B.R. performed the experiments and analysed the data; D.B. and R.B.R. wrote the manuscript; and all authors edited and approved the manuscript.

Funding

This work was supported by research grant R01 DE024942 (RBR) and S10 OD025246 (DAF) from the National Institutes of Health, and Pathology Department Doisy Research Seed Grant (RBR).

Data availability

No datasets were generated or analysed during the current study.

Declarations

Consent for publication

Not applicable.

Competing interests

The authors declare no competing interests.

Author details

¹Department of Pathology, Saint Louis University, 1100 South Grand Boulevard, St. Louis, MO 63104, USA. ²Biochemistry & Molecular Biology, Saint Louis University, St. Louis, MO, USA. ³Department of Chemistry and Medicine, Washington University, St. Louis, MO, USA. ⁴Center of Mass Spectrometry and Metabolic Tracing, Washington University, St. Louis, MO, USA. ⁵Department of Otolaryngology, Head and Neck Surgery, Harvard Medical School, Massachusetts Eye and Ear, Boston, MA, USA.

Received: 12 August 2024 Accepted: 20 November 2024

Published online: 18 December 2024

References

- Chelakkot C, Chelakkot VS, Shin Y, Song K. Modulating glycolysis to improve cancer therapy. *Int J Mol Sci.* 2023;24(3):2606.
- Ganapathy-Kanniappan S, Geschwind JF. Tumor glycolysis as a target for cancer therapy: progress and prospects. *Mol Cancer.* 2013;12:152.
- Feng Y, Xiong Y, Qiao T, Li X, Jia L, Han Y. Lactate dehydrogenase A: A key player in carcinogenesis and potential target in cancer therapy. *Cancer Med.* 2018;7(12):6124–36.
- Sur S, Nakanishi H, Flaveny C, Ippolito JE, McHowat J, Ford DA, et al. Inhibition of the key metabolic pathways, glycolysis and lipogenesis, of oral cancer by bitter melon extract. *Cell Commun Signal.* 2019;17(1):131.
- Broadfield LA, Pane AA, Talebi A, Swinnen JV, Fendt SM. Lipid metabolism in cancer: New perspectives and emerging mechanisms. *Dev Cell.* 2021;56(10):1363–93.
- Zhang C, Zhu N, Li H, Gong Y, Gu J, Shi Y, et al. New dawn for cancer cell death: Emerging role of lipid metabolism. *Mol Metab.* 2022;63: 101529.
- Lemberg KM, Gori SS, Tsukamoto T, Rais R, Slusher BS. Clinical development of metabolic inhibitors for oncology. *J Clin Invest.* 2022;132(1):e148550.
- Sur S, Ray RB. Bitter melon (*Momordica Charantia*), a nutraceutical approach for cancer prevention and therapy. *Cancers (Basel).* 2020;12(8):2064.
- Fazel MF, Abu IF, Mohamad MHN, Mat Daud NA, Hasan AN, Aboo Bakkar Z, et al. Physicochemistry, Nutritional, and Therapeutic Potential of *Ficus carica* - A Promising Nutraceutical. *Drug Des Devel Ther.* 2024;18:1947–68.

10. Malathi N, Rajan ST, Warnakulasuriya S. Natural products and diet for the prevention of oral cancer: Research from south and southeast Asia. *Oral Dis*; 2024. <https://doi.org/10.1111/odi.15002>. Epub ahead of print.
11. Cao N, Li X, Zhang W, Wang Q, Liang Y, Zhou F, et al. Research progress of signaling pathways of the natural substances intervene dyslipidemia (Review). *Exp Ther Med*. 2022;24(2):494.
12. Sur S, Steele R, Isbell TS, Venkata KN, Rateb ME, Ray RB. Momordicine-I, a bitter melon bioactive metabolite, displays anti-tumor activity in head and neck cancer involving c-met and downstream signaling. *Cancers (Basel)*. 2021;13(6):1432.
13. Kao Y, Chou CH, Huang LC, Tsai CK. Momordicine I suppresses glioma growth by promoting apoptosis and impairing mitochondrial oxidative phosphorylation. *EXCLI J*. 2023;22:482–98.
14. Sur S, Bhartiya P, Steele R, Brennan M, DiPaolo RJ, Ray RB. Momordicine-I Suppresses Head and Neck Cancer Growth by Reprogramming Immunosuppressive Effect of the Tumor-Infiltrating Macrophages and B Lymphocytes. *Mol Cancer Ther*. 2024;23(5):672–82.
15. Adams KJ, Pratt B, Bose N, Dubois LG, St John-Williams L, Perrott KM, et al. Skyline for Small Molecules: A Unifying Software Package for Quantitative Metabolomics. *J Proteome Res*. 2020;19(4):1447–58.
16. Zambrano A, Molt M, Uribe E, Salas M. Glut 1 in Cancer Cells and the Inhibitory Action of Resveratrol as A Potential Therapeutic Strategy. *Int J Mol Sci*. 2019;20(13):3374.
17. Yang H, Zhong JT, Zhou SH, Han HM. Roles of GLUT-1 and HK-II expression in the biological behavior of head and neck cancer. *Oncotarget*. 2019;10(32):3066–83.
18. Liu S, Liu W, Ding Z, Yang X, Jiang Y, Wu Y, et al. Identification and validation of a novel tumor driver gene signature for diagnosis and prognosis of head and neck squamous cell carcinoma. *Front Mol Biosci*. 2022;9:912620.
19. Chan CY, Hong SC, Chang CM, Chen YH, Liao PC, Huang CY. Oral squamous cell carcinoma cells with acquired resistance to erlotinib are sensitive to anti-cancer effect of quercetin via Pyruvate Kinase M2 (PKM2). *Cells*. 2023;12(1):179.
20. Chen F, Tang C, Yang F, Ekpenyong A, Qin R, Xie J, et al. HSP90 inhibition suppresses tumor glycolytic flux to potentiate the therapeutic efficacy of radiotherapy for head and neck cancer. *Sci Adv*. 2024;10(8):eadk3663.
21. Zhang L, Liu X, Liu Y, Yan F, Zeng Y, Song Y, et al. Lysophosphatidylcholine inhibits lung cancer cell proliferation by regulating fatty acid metabolism enzyme long-chain acyl-coenzyme A synthase 5. *Clin Transl Med*. 2023;13(1):e1180.
22. Loos B, du Toit A, Hofmeyr JH. Defining and measuring autophagosome flux-concept and reality. *Autophagy*. 2014;10(11):2087–96.
23. Zhang YB, Gong JL, Xing TY, Zheng SP, Ding W. Autophagy protein p62/SQSTM1 is involved in HAMLET-induced cell death by modulating apoptosis in U87MG cells. *Cell Death Dis*. 2013;4(3):e550-e.
24. Muhammad N, Steele R, Isbell TS, Phillips N, Ray RB. Bitter melon extract inhibits breast cancer growth in preclinical model by inducing autophagic cell death. *Oncotarget*. 2017;8(39):66226–36.
25. Yun HM, Kwon YJ, Kim E, Chung HJ, Park KR. Machilin D promotes apoptosis and autophagy, and inhibits necroptosis in human oral squamous cell carcinoma cells. *Int J Mol Sci*. 2023;24(5):4576.
26. Young MM, Takahashi Y, Khan O, Park S, Hori T, Yun J, et al. Autophagosomal membrane serves as platform for intracellular death-inducing signaling complex (iDISC)-mediated caspase-8 activation and apoptosis. *J Biol Chem*. 2012;287(15):12455–68.
27. Szablewski L. Expression of glucose transporters in cancers. *Biochim Biophys Acta*. 2013;1835(2):164–9.
28. Barron CC, Bilan PJ, Tsakiridis T, Tsiani E. Facilitative glucose transporters: Implications for cancer detection, prognosis and treatment. *Metabolism*. 2016;65(2):124–39.
29. Hsu MC, Hung WC. Pyruvate kinase M2 fuels multiple aspects of cancer cells: from cellular metabolism, transcriptional regulation to extracellular signaling. *Mol Cancer*. 2018;17(1):35.
30. Strickland M, Stoll EA. Metabolic Reprogramming in Glioma. *Front Cell Dev Biol*. 2017;5:43.
31. Kim B, Lee HS, Kim HJ, Lee H, Lee IY, Ock S, et al. Momordica charantia (bitter melon) efficacy and safety on glucose metabolism in Korean prediabetes participants: a 12-week, randomized clinical study. *Food Sci Biotechnol*. 2023;32(5):697–704.
32. Lei G, Zhuang L, Gan B. Targeting ferroptosis as a vulnerability in cancer. *Nat Rev Cancer*. 2022;22(7):381–96.
33. Abraham M, Sowmya S, Rao RS, Haragannavar VC, Patil S, Augustine D, et al. Stearoyl coenzyme A desaturase: a diagnostic and prognostic biomarker in patients with oral epithelial dysplasia and oral squamous cell carcinoma. *Transl Res Oral Oncol*. 2018;3:2057178X18782512.
34. Liu P, Zhu W, Chen C, Yan B, Zhu L, Chen X, et al. The mechanisms of lysophosphatidylcholine in the development of diseases. *Life Sci*. 2020;247:117443.
35. Ross T, Jakubzig B, Grundmann M, Massing U, Kostenis E, Schlesinger M, et al. The molecular mechanism by which saturated lysophosphatidylcholine attenuates the metastatic capacity of melanoma cells. *FEBS Open Bio*. 2016;6(12):1297–309.
36. Wen H, Zhou S, Song J. Induction of apoptosis by magnolol via the mitochondrial pathway and cell cycle arrest in renal carcinoma cells. *Biochem Biophys Res Commun*. 2019;508(4):1271–8.
37. Cardoso SM, Rego AC, Penacho N, Oliveira CR. Apoptotic cell death induced by hydrogen peroxide in NT2 parental and mitochondrial DNA depleted cells. *Neurochem Int*. 2004;45(5):693–8.
38. Onyango IG, Khan SM. Oxidative stress, mitochondrial dysfunction, and stress signaling in Alzheimer's disease. *Curr Alzheimer Res*. 2006;3(4):339–49.
39. Matsuura K, Canfield K, Feng W, Kurokawa M. Metabolic Regulation of Apoptosis in Cancer. *Int Rev Cell Mol Biol*. 2016;327:43–87.
40. Lieu EL, Nguyen T, Rhyne S, Kim J. Amino acids in cancer. *Exp Mol Med*. 2020;52(1):15–30.
41. Lin SR, Fu YS, Tsai MJ, Cheng H, Weng CF. Natural compounds from herbs that can potentially execute as autophagy inducers for cancer therapy. *Int J Mol Sci*. 2017;18(7):1412.
42. Al-Bari MAA, Ito Y, Ahmed S, Radwan N, Ahmed HS, Eid N. Targeting autophagy with natural products as a potential therapeutic approach for cancer. *Int J Mol Sci*. 2021;22(18):9807.
43. Eltayeb K, La Monica S, Tiseo M, Alfieri R, Fumarola C. Reprogramming of lipid metabolism in lung cancer: an overview with focus on EGFR-mutated non-small cell lung cancer. *Cells*. 2022;11(3):413.
44. Yang S, Hu C, Chen X, Tang Y, Li J, Yang H, et al. Crosstalk between metabolism and cell death in tumorigenesis. *Mol Cancer*. 2024;23(1):71.

Publisher's Note

Springer Nature remains neutral with regard to jurisdictional claims in published maps and institutional affiliations.